Scholars Journal of Engineering and Technology (SJET) **ISSN 2347-9523 (Print)**
Abbreviated Key Title: Sch. J. Eng. Tech. **ISSN 2321-435X (Online)**

A Unit of Scholars Academic and Scientific Society, India
www.saspublisher.com

Effects of Heat Cambering On Residual Stresses in Steel Beams

Shaban Salem[2*], Keith Kowalkowski, Ph.D, PE, SE[2]
[2]PhD Candidate, Lawrence Technological University, Southfield, Michigan
[2]Associate Professor of Civil Engineering, Lawrence Technological University, Southfield Michigan

Original Research Article

***Corresponding author**
Shaban Salem

Article History
Received: 04.04.2018
Accepted: 14.04.2018
Published: 30.04.2018

DOI:
10.21276/sjet.2018.6.4.1

Abstract: Cambering is used to offset the downward deflections in steel beams due to gravity loads by producing an initial upward camber and a curved shape. Two methods can be used to perform cambering; (1) cold cambering and (2) heat cambering. Research has shown that significant residual stresses develop in the cross-section when cambering that may influence the structural performance upon further loading. An extensive research project was performed to evaluate the influence of both cold and heat cambering on such residual stresses. Experimentally, cold cambering was achieved by creating significant plastic deformations in steel beams using a hydraulic actuator. Heat cambering was achieved by applying Vee heats to the web and strip heats to the flange at intervals along the length of the steel beams. This caused yielding in the heated regions at high temperatures due to restraint from the unheated material. In both cases, residual stresses were measured after the completion of the tests. Finite element models were developed for both cold-cambered and heat-cambered beams to further investigate the development and patterns of residual stresses. Heating cycles were simulated in the finite element models using time-temperature curves generated using a heat transfer analysis performed with the finite difference method. Experimental and analytical residual stress results compared favorably well to each other. Results indicated that cold-cambering does not cause a major concern with respect to residual stresses. The results indicate that residual stresses in heat-cambered are significant, reaching or exceeding the yield stress. The residual stress results are much higher than assumed in AISC equations used to predict the moment capacity of steel beams. However, the results indicate that high stresses are localized near the heated area and thus, the stresses only have a small influence on the load-displacement behavior of steel beams under further loading.
Keywords: Cold-Cambering, Heat-Cambering, Heat Transfer Analysis, Residual Stresses, Finite Element Analysis, Finite Difference Method, Steel Beams.

INTRODUCTION

Cambering is used to reduce the downward deflection in steel beams part by producing an upward camber and a curved shape. The amount of camber specified usually offsets the dead load deflections and in some instances offsets the dead loads and a portion of the live load. Most steel beams within building systems are designed assuming they are subjected to a uniformly distributed load or point loads along the length similar to uniformly distributed loads. Deflected shapes are parabolic and camber provides a reverse parabola by curving the beams in the opposite direction.

There are two methods available for cambering steel beams: (1) cold-cambering and (2) heat-cambering. Cold-cambering is more common and accomplished by applying mechanical forces to induce permanent inelastic (material reaches stresses beyond yield stress) deformations using specialized equipment. The equipment generally consists of a large rigid frame by which the beam can be mounted horizontally with loads applied to one side of the flange using a single ram or double ram system while the side of the flange is supported. Figure-1 shows an illustration of the cold-cambering method using a double ram configuration [1].

Heat-cambering is performed by applying heat with a torch to the flange and the web at various points along the length and in specific patterns. During each heat, the member starts to bend in the direction opposite to the intended direction from thermal expansion. Then, the beam will bend in the desired direction when it completely has cooled [2]. Heat-cambering is more of a trial and error process because it is not possible to measure the required camber until the beam has cooled [1]. In addition, more labor is required to heat-camber as opposed to cold-camber.

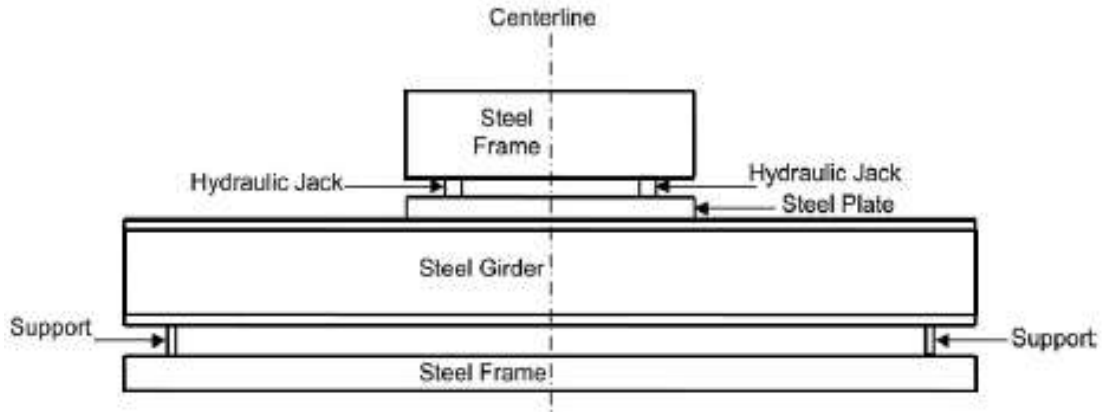

Fig-1: Layout of the frame and cambering equipment [1]

Heat-cambering is often used when the depth of the beam is greater than the capacity of cold cambering [3]. Thermal stresses have been used for cambering or curving by steel fabricators since the 1930's and the usage has increased steadily since that time [4]. In this process, "Vee" heats are applied to the web of the steel beam followed by strip heats applied to the flange at the open end of the Vee.

Heat-straightening is similar to heat-cambering with respect to how heat is applied and heating patterns but is often used to repair a beam to have its original configuration prior to damage [5]. Early heat-straightening repairs were conducted with limited research on its influence on material properties and residual stresses. Early research studies focused on understanding the thermal expansion properties of the steel [6-8] and general procedures for application [9]. The damage of steel members usually comes from fire, wind, earthquake, and overloading [5]. It is frequently used by various DOTs (Department of Transportation) around the country for damaged steel fascia beams. Heat-straightening is fundamentally different than heat-cambering as it involves plastic damage followed by heating repair and often includes a restraining force to assist in forcing the steel back to its original configuration. However, heat-cambering and heat-straightening are both used to induce deformations in structural steel shapes.

The influence of heat-straightening on residual stresses was studied by Charles Roeder at the University of Washington [10, 4]. Roeder used the finite element model to predict the residual stresses in a plate element subjected to Vee heats. Avent *et al*., [11] investigated the effects of heat straightening on the residual stress distribution in A36 steel plates. The results from this study indicated that both the undamaged and damaged plates exhibited similar residual stress distributions as Roeder's [10]. Avent *et al.*, [12] conducted experimental investigations to investigate the effects of the Vee angle on induced residual stresses of heat-straightened plates. The experimental results indicated that larger Vee angles produced slightly higher residual stresses in the cross-section.

Kowalkowski [5] has shown using the finite element method that damage followed by heating repairs (heat-straightening) can cause significant residual stresses in steel beams, which causes a concern in structural performance under service loads. Therefore, heat-cambering will likely cause significant residual stresses as well developing similar concerns for the structural performance in steel buildings. Because of this, an extensive experimental and analytical research program was performed to identify the magnitude of residual stresses in steel beams from cold-cambering and heat-cambering and for further analyzing the beams under service loads.

EXPERIMENTAL INVESTIGATIONS

Laboratory-scale beams were cambered by cold-cambering and heat-cambering. All experimental investigations were performed in the Structural Testing Center (STC) at Lawrence Technological University (LTU). Two steel beams were subjected to cold-cambering and three steel beams were subjected to heat-cambering. The two cold-cambered beams were the same wide-flange shape as two heat-cambered beams and slated to be subjected to the same nominal maximum camber as the heat-cambered beams.

Experimental Investigations of Cold-Cambered Beams

Two experimental tests were carried out on steel beams that were cold-cambered. Both beams were fabricated from ASTM A992 steel. One steel beam was a W8X18 and the other was a W14X30. The primary objectives of these experimental investigations were to evaluate the residual stresses but more importantly to compare the results vs. the results of finite element models and the experimental results of heat-cambered beams.

Figure-2 shows an illustration of the test setup used for the cold-cambering procedure. The steel beam specimen was supported vertically by two 3 in. diameter cylinders to allow free rotation at either end. The beam specimens had a total length of 17 ft. and a length between the support centerlines of 15 ft. The steel cylinders were placed on two steel HSS steel tubes to increase the elevation of the beam specimens and to ensure free rotation at each support. The steel tubes were placed on steel supports that were 30 in. in height above the ground. Load was applied at midspan by a hydraulic actuator with a capacity of 55 kips. The actuator was connected to a steel loading frame. Load was measured using a load cell and displacement was measured at midspan using a displacement transducer. Camber was measured as the midspan displacement after load was removed from the steel beam, thus representing the permanent or plastic deformation of the beam. Two steel plates (10 in. x 5 in. x 1 in. and 10 in. x 10 in. x 2 in.) and one HSS steel tube (HSS6X6X1/2) were placed between the actuator and the top flange of the steel beam to simulate the load.

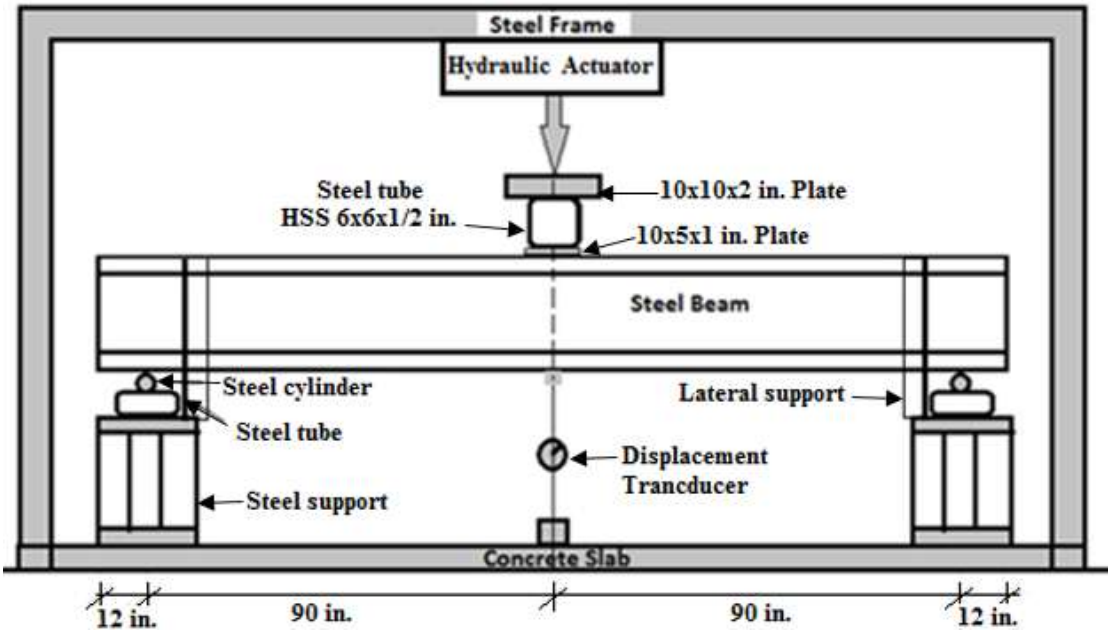

Fig-2: Experimental setup for cold-gambered beams

Experimental Investigations of Heat-Cambered Beams

Laboratory-scale beam specimens were cambered by heat-cambering using oxy-acetylene torches. The primary objectives were to determine the residual stresses that develop in heat-cambered beams, compare the results to the residual stresses that develop in cold-cambered beams, and to compare the results to the residual stresses obtained from finite element models of heat-cambered beams.

All beams subjected to heat-cambering were placed on the same end supports as used for cold-cambering and tested on the loading dock adjacent to the STC. A photograph of the test setup is shown in Figure-3.

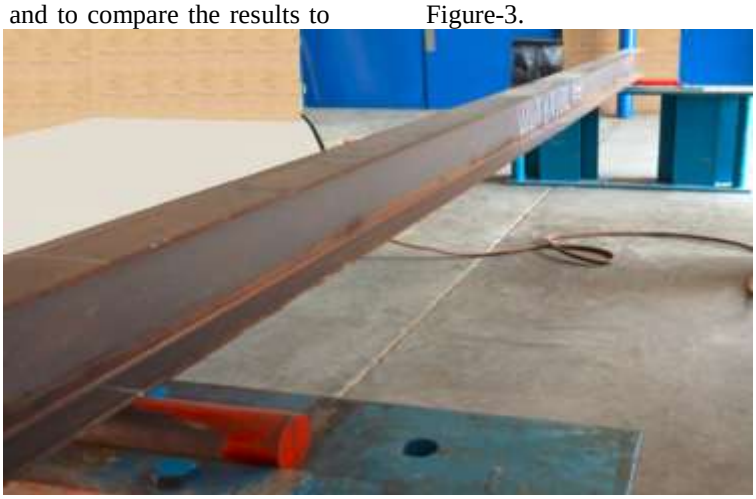

Fig-3: Test setup for heat-cambered beams on loading dock of STC

Two W8X18 beams were heat-cambered. The first was heat-cambered to 0.82 in. and the other was heat-cambered to 1.5 in. Heat-cambering was conducted by first Vee heating the web from both sides simultaneously. Therefore, two torches were used to conduct the Vee heating to produce a uniform temperature through the thickness of the web. The depth of each Vee was 5.61 in. which corresponds to a depth ratio of 0.5, and the width of each Vee was 4.64 in., which corresponds to a Vee angle of 45°. Initially, a spot heat was applied to the apex of the Vee until the temperature reached 1200 °F. Then, the torches were moved in serpentine paths from the apex of the Vee to the top of the Vee holding the temperature near the torch as close to 1200 °F as possible. Directly after the Vee heat was completed, one torch was used to apply strip heats to the top flange with a strip length of 4.64 in. along the length of the beam and across the entire flange width. The temperature of the steel surface was monitored using an infrared temperature gun as shown in Figure-4. One researcher monitored the temperature and communicated with the researcher on the opposite side when Vee heats were applied to the web.

Fig-4: Infrared temperature gun used to measure steel temperature

After each heating cycle (combination of Vee and strip heat), the heated region was cooled to a temperature of 250°F prior to applying heat to another location. The beam camber was measured in between each heating cycle using a measuring tape. The distance from the ground to the bottom of the beam at midspan was measured prior to applying any heating cycles and then, the same distance was measured after each heating cycle. The difference between the original measurement and measurement after each heating cycle was the total camber achieved.

The locations of the Vee heats and strip heats were marked on the beam prior to conducting any heating cycles. The Vee heat locations were designed such that they partially overlap, similar to that used in previous research performed by Kowalkowski [5]. The nomenclature used for the location of each Vee heat is illustrated in Figure-5. The Vee heat located at midspan was identified as C; the Vee heats on one side of midspan were identified as R1, R2, R3 (etc.); and the Vee heats on the other side of midspan were identified as L1, L2, L3 (etc.).

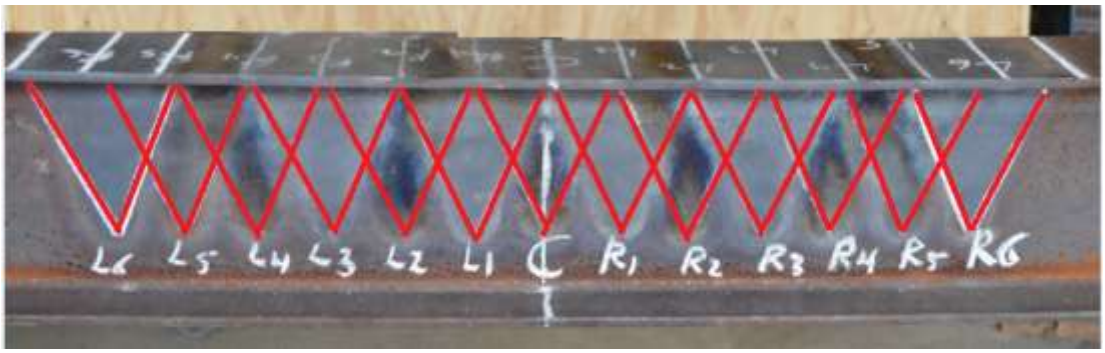

Fig-5: Nomenclature/location of Vee heats applied to W8X18 beam specimen

One W14X30 beam specimen was heat-cambered to a maximum camber of 1.5 in. at midspan. The depth of each Vee heat was 6.52 in. which corresponds to a depth ratio of 0.5, and the width of each Vee heat was 5.40 in., which corresponds to a Vee angle of 45°. A description of the heating procedure is similar to that described for the W8X18 beams except two torches were used to apply the strip heat to the top flange, which was always located directly above the Vee heats during the same heating cycle.

The nomenclature used for each Vee/strip heat was the same as the nomenclature used for the W8X18 beam specimens. However, the depth and width of the Vee heats were different. Figure-6 shows the locations of the Vee heats marked on the W14X30 beam specimen.

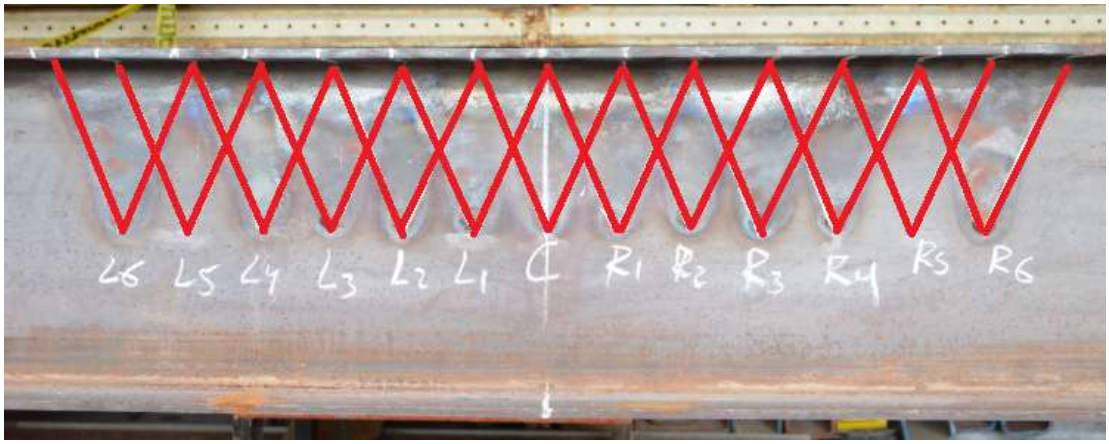

Fig-6: Nomenclature/location of Vee heats applied to W14X30 beam specimen

Camber Deformations Achieved per Heating Cycle

Heating cycles were applied using the nomenclature of the Vee/strip heats identified in Figures 5 and 6. The first W8X18 beam specimen was subjected to heating cycles until the final camber was 0.82 in. The second W8X18 beam was subjected to heating cycles until the final camber was 1.5 in. The W14X30 beam was subjected to heating cycles until the final camber was 1.5 in. Table-1 summarizes the sequence of Vee/strip heats used, the amount of total camber achieved after each heating cycle, and the incremental camber achieved after each heating cycle. Seven heating cycles were required to camber the first W8X18 beam to 0.82 in. Significant camber (33% of the total camber) was achieved in the second and fourth heating cycle. For the second W8X18 beam, twenty-two heating cycles were required to produce 1.5 in. camber. A similar amount of incremental camber was achieved during each heating cycle for this beam specimen. For the W14X30 beam, twenty-six heating cycles were required to camber the beam to 1.5 in. Each Vee/strip heat location needed to be heated exactly twice.

After reviewing all of the results, it appears that the average amount of camber achieved in a heating cycle is approximately 0.08 in. It is also anticipated that if the incremental camber is significantly higher, the steel was overheated during the cycle. The results are more varied for the first W8X18 beam specimen, which is logical as the researchers were getting used to the testing procedure. If the amount of camber achieved in a heating cycle was significantly lower than 0.08 in., it is likely that not enough heat was applied to the Vee/strip region.

Table-1: Heat-cambering sequence and camber magnitude for steel beam specimens

	W8X18 Beam 1			W8X18 Beam 2			W14X30		
Heat cycle	Vee/Strip Location	Total Camber (in.)	Increm. Camber (in.)	Vee/Strip Location	Total Camber (in.)	Increm. Camber (in.)	Vee/Strip Location	Total Camber (in.)	Increm. Camber (in.)
Heat 1	C	0.08	0.08	C	0.08	0.08	C	0.04	0.04
Heat 2	L2	0.27	0.19	L2	0.16	0.08	L2	0.12	0.08
Heat 3	R2	0.39	0.12	R2	0.24	0.08	R2	0.2	0.08
Heat 4	L4	0.55	0.16	L4	0.31	0.07	L4	0.31	0.11
Heat 5	R4	0.63	0.08	R4	0.39	0.08	R4	0.43	0.12
Heat 6	L1	0.75	0.12	L1	0.47	0.08	L1	0.45	0.02
Heat 7	R1	0.82	0.07	R1	0.47	0	R1	0.47	0.02
Heat 8				C	0.55	0.08	L3	0.51	0.04
Heat 9				L2	0.63	0.08	R3	0.55	0.04
Heat 10				R2	0.71	0.08	L6	0.59	0.04
Heat 11				L4	0.73	0.02	R6	0.63	0.04
Heat 12				R4	0.75	0.02	L5	0.71	0.08
Heat 13				L1	0.83	0.08	R5	0.79	0.08
Heat 14				R1	0.91	0.08	C	0.87	0.08
Heat 15				L3	0.98	0.07	L2	0.91	0.04
Heat 16				R3	1.02	0.04	R2	0.94	0.03
Heat 17				L5	1.1	0.08	L4	1.02	0.08
Heat 18				R5	1.18	0.08	R4	1.1	0.08
Heat 19				L6	1.26	0.08	L1	1.1	0
Heat 20				R6	1.34	0.08	R1	1.14	0.04
Heat 21				L3	1.42	0.08	L3	1.14	0
Heat 22				R3	1.5	0.08	R3	1.18	0.04
Heat 23							L6	1.26	0.08
Heat 24							R6	1.34	0.08
Heat 25							L5	1.42	0.08
Heat 26							R5	1.5	0.08

Figure-7 shows the relationship between the number of heating cycles and the camber achieved for the three beam specimens. As shown, the first W8X18 beam specimen achieved more camber in early heating cycles in comparison to the second beam. This may be slightly attributed to the higher elastic modulus measured for the first beam but more likely due to average temperature in the heated region during various heating cycles. However, for both W8X18 beam specimens, the relationship identified in Figure-7 is fairly linear. For the W14X30 beam, Figure-7 shows a non-linear relationship for camber achieved in each heating cycle. After further inspection of the results, on average, a small decrease in camber was achieved when Vee/strip heats were applied to the same location twice per the nomenclature in Figure-6. Overall, the amount of camber achieved in each heating cycle for all beam specimens is very dependent on the amount of overall heat applied in a particular cycle.

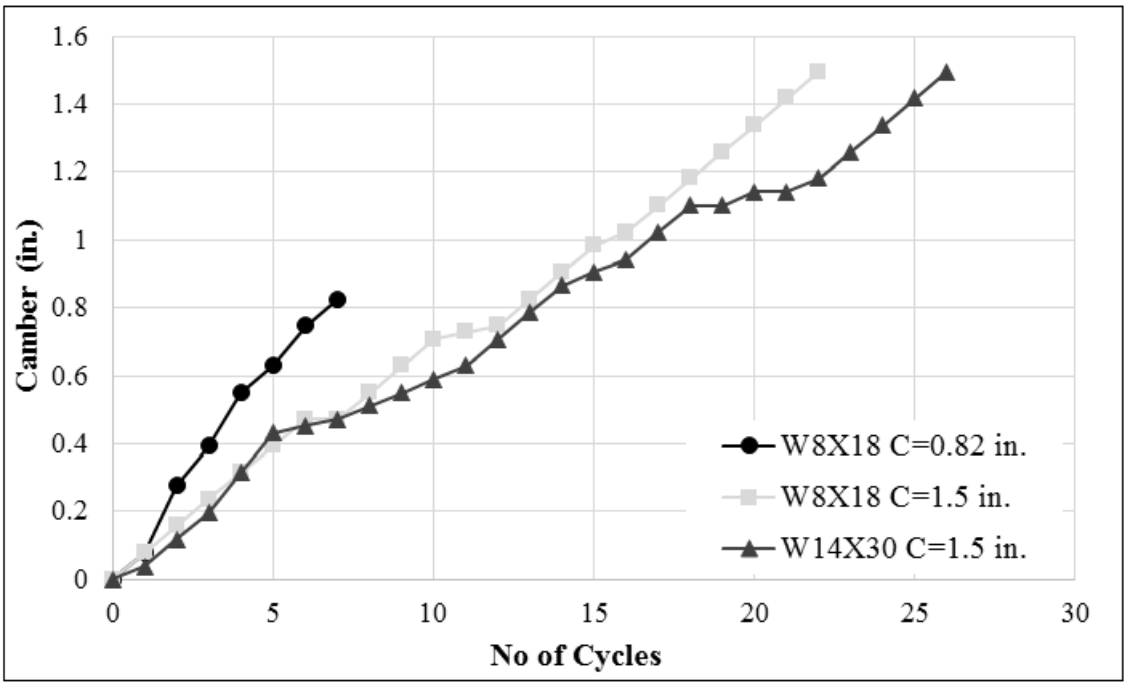

Fig-7: Relationship between the heating cycles and the total camber

Measurement of Residual Stresses

Residual stresses in cambered beams were measured within the center 3 ft. of the beams in three sections of 1 ft. each using the sectioning method. In this method, the distance between two points in a strip are measured before cutting and after cutting out the individual strip. Residual strains are measured first as the change in length between the points divided by the original distance between points and residual stresses are determined using the stress-strain curves measured for each experimental beam. Of the three sections, the section directly at midspan was identified as "Middle" and the sections on either side were identified as "Left" and "Right". Prior to cutting the sections out, DEMEC dots were glued within the sections and along the flange and web at a spacing of 8 in. as shown in Figure-8. Therefore, the section in which the residual stresses were measured from was 4 in. longer than the distance between dots and residual stress measurements are averaged over the 8 in. length of material. Between strips, the dots were placed between 0.375 in. and 0.75 in. apart. Therefore, each strip that was removed from the beam specimen was between 0.375 in. to 0.75 in. wide with the dots located at the center of the strip. The distance between the dots were measured before and after the fabrication of the strips using a DEMEC device as shown in Figure-8. The instrument has a precision of 0.001 mm.

Fig-8: Photograph showing measurement between dots using the DEMEC device

Residual Stress Results in Experimental Beams

Residual stress results for cold-cambered beams were not as relevant in this study as they were used for comparison purposes only. They are presented in detail elsewhere [13]. For all cold-cambered and heat-cambered beams, residual stresses were measured

in the top flange which was the flange heated with strip heats, in the web, and in the bottom flange. The residual stress results from the unheated bottom flange are presented elsewhere [13].

Figure-9 shows the residual stress results in the web of the first W8X18 beam heat-cambered to 0.82 in. and in all three sections mentioned. Note that the stresses are averaged in an 8 in. length in which they are measured. Figure-9 indicates that the residual stress patterns are very similar in all three sections. However, there are noticeable differences in the magnitudes. The residual stresses are primarily tension. The last Vee heat was applied at location R1 from Figure-5. This is located within the middle section, which is likely related to why the final residual stresses are highest in the middle section.

Figure-10 shows the residual stresses in the top flange of the first W8X18 beam heat cambered to 0.82 in. and in all three sections mentioned as a function of flange width. In all three sections, the residual stress results are primarily compression. However, the residual stresses are higher tension near the center or k-region of the beam. This compares well with the results of the residual stresses in the web from Figure-9 where the residual stresses at the very top of the web are tension, yet smaller in comparison to the tensile residual stresses in the rest of the web. In Figure 10, the residual stresses are more compressive near the tips of the flanges. This is expected since the tips of the flanges cool faster causing higher tensile yielding upon initial cooling which results in a compressive stress upon final cooling as the cross-section tries to become plane when it cools to ambient temperatures. The results of the left and right sections are very similar which indicates a favorable result. The left and right sections of the beam were only directly heated when heats were applied to L4 and R4. This is likely related to why they have less residual stresses in comparison to the middle section.

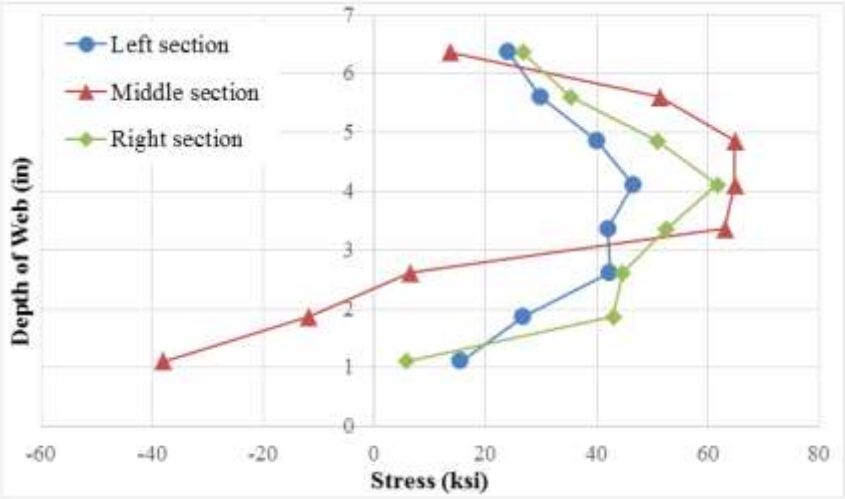

Fig-9: Residual stresses in the web of the W8X18 heat-cambered to 0.82 in

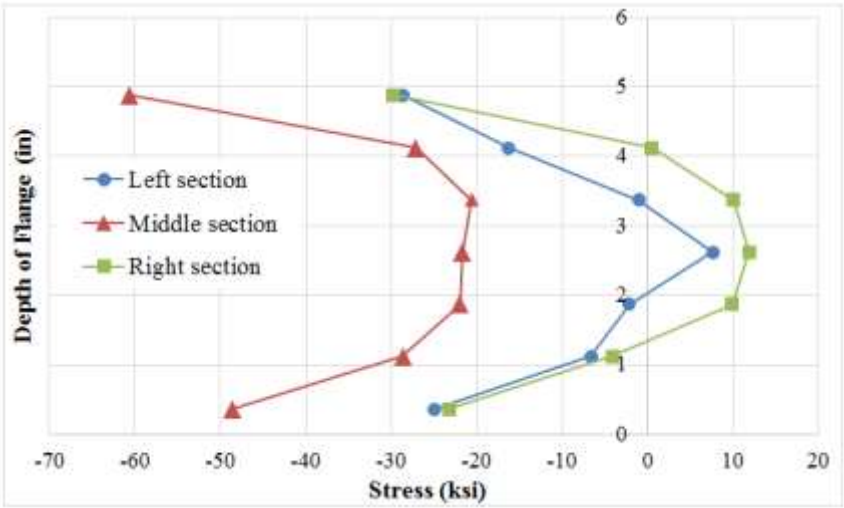

Fig-10: Residual stresses in the top flange of the W8X18 heat-cambered to 0.82 in

Figure-11 shows the residual stress results in the web of the second W8X18 beam heat cambered to 1.5 in as a function of the web depth. The shape of the curve is not as favorable as for the W8X18 beam heat cambered to 0.82 in. from Figure 9. Instead, the results appear more random. However, a lot more heating cycles were required to camber the second beam and in some cases, the area where the residual stress was measured was heated twice. Overall, it took 7 heating cycles to camber the first beam and 22 heating cycles to camber the second beam. This may cause more fluctuations in the residual stresses within the 8 in. lengths of the individual strips. Similar to the first beam, the residual stresses are primarily tension with the exception of the bottom of the web, where some of the residual stress results are compression near the bottom flange. The results also indicate that a significant depth of the web had high residual stresses near the yield stress of the material, which was measured experimentally as 65.9 ksi.

Figure-12 shows the residual stresses in the top flange of the second W8X18 beam heat cambered to 1.5 in. as a function of flange width. Figure 12 shows a random distribution of the residual stress pattern in the middle section and shows similar patterns in the left and right sections. Similar to the beam heat cambered to 0.75 in., the residual stresses in the top flange are primarily compression. Therefore, overall, even though the residual stress results appear more random, general comparisons between the heat-cambered beams can be made for both the results in the web and in the top flange.

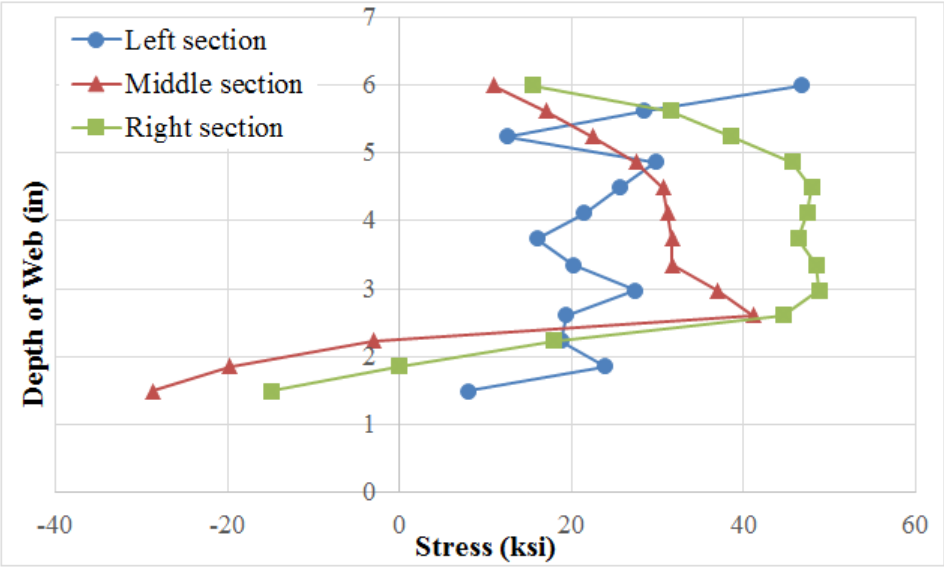

Fig-11: Residual stresses in the web of the W8X18 heat-cambered to 1.5 in

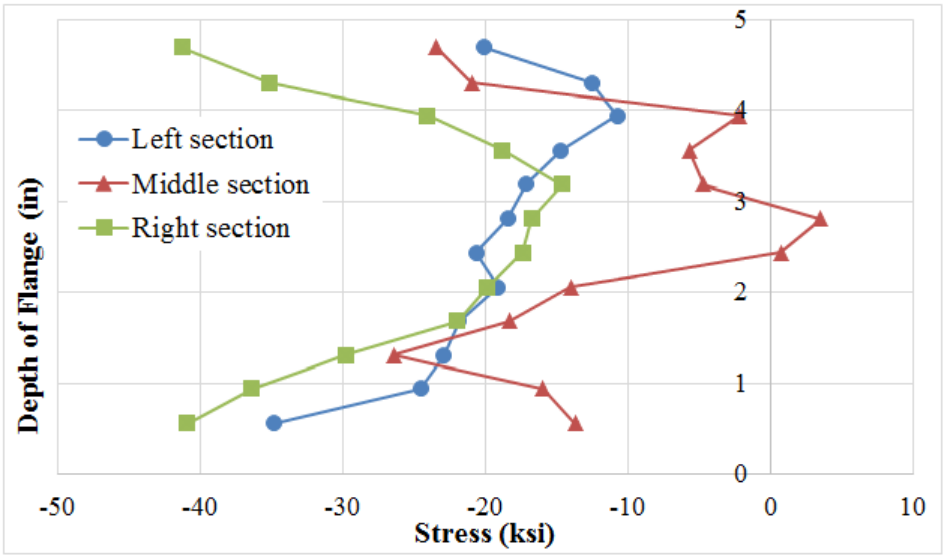

Fig-8: Residual stresses in the top flange of the W8X18 heat-cambered to 1.5 in.

Figure-13 shows the residual stress results in the web of the W14X30 beam heat-cambered to 1.5 in. as a function of the web depth. Note that 0.75 in. individual wide strips were removed for each set of dots in lieu of the 0.375 in. and 0.75 in. wide strips removed for the W8X18 beams.

The residual stress results in Figure-13 are random and do not provide clear conclusions with respect to typical residual stress patterns that develop in heat-cambered beams. One downfall of the procedure is that residual stresses are averaged in an 8 in. strip instead of in more localized region. It is anticipated from equilibrium conditions, that the net stress in one cross-section is zero and smooth transitions in the residual stress magnitudes exist from one point to the next in a cross-section. However, a significant amount of variation can occur in the length measured. The variation in residual stresses may also be due to the heating conditions for each section. Overall, 26 heating cycles were required to camber the beam to the desired amount and individual Vee heat locations were heated multiple times. The results show values exceeding the yield stress and it is probable that in more localized locations, the residual stresses significantly exceed the yield stress.

Figure-14 shows the residual stresses in the top flange of the W14X30 beam heat cambered to 1.5 in. as a function of flange width. All the flange sections show similar behavior in the residual stress patterns except at one edge of the middle section, which has an irregular result. However, the middle section was primarily tension after the experimental investigations and the left and right sections were primarily compression. Overall, the results in the top flange was more favorable than the results in the web and are more valuable in predicting the behavior of residual stresses in steel shapes subjected to heat-cambering. The left and right sections compare more favorably to the W8X18 beams in which compressive residual stresses were primarily measured in the flanges. In general, all three results show more compressive stresses near the tips of the flange, which is similar to both W8X18 beams and expected since the tips of the flanges are expected to cool faster at higher temperatures.

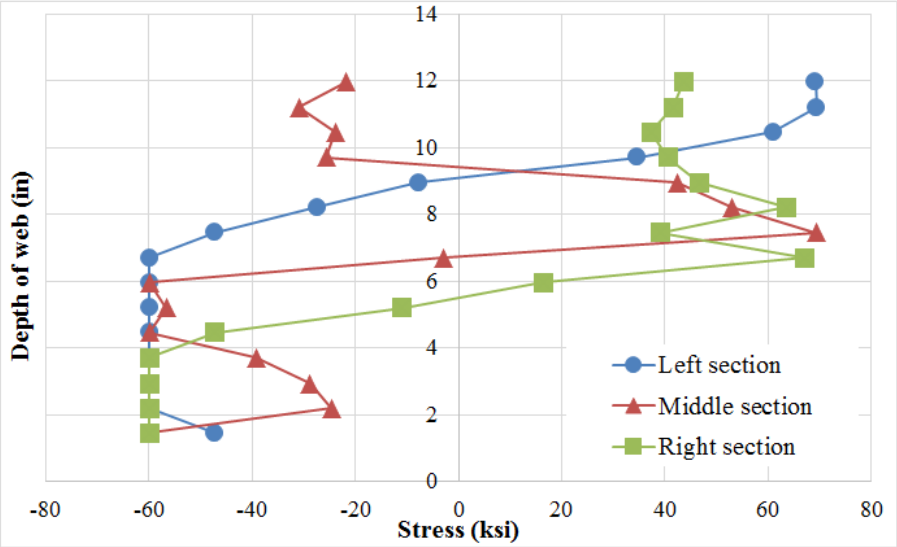

Fig-9: Residual stresses in the web of the W14X30 heat-cambered beam

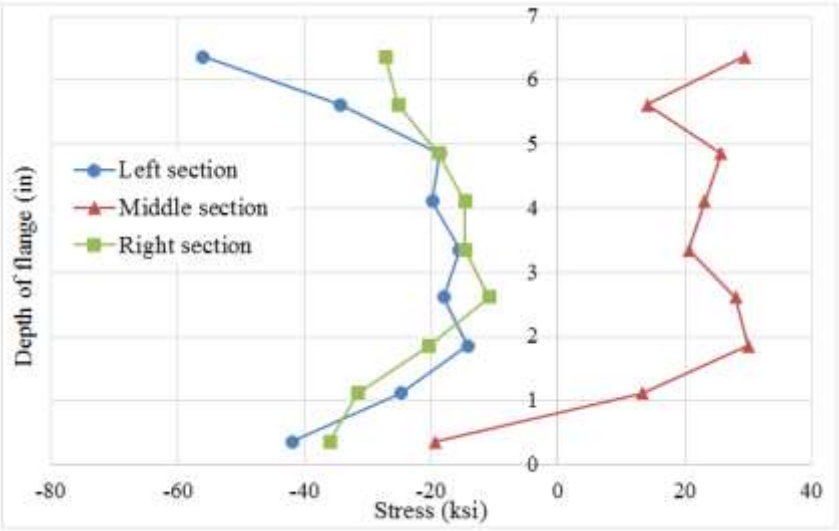

Fig-10: Residual stresses in the top flange of the W14X30 heat-cambered beam

ANALYTICAL RESULTS

Analytical investigations were performed using the finite element method and the finite element software ABAQUS [14]. This section summarizes all the finite element results of a model developed to represent the first W8X18 beam, which was heat-cambered to 0.82 in. Detailed graphs from the finite element models are provided for this beam. The residual stresses from finite element models developed for the other two experimental beams are discussed in this section as well. Additional heat-cambered beams with various sizes, boundary conditions, and magnitudes of camber were also modeled using finite element models and are discussed in detail in Salem [13].

Initial finite element models of cold and heat-cambered beams were used to verify the boundary conditions and loading conditions used in all finite element models. For instance, the finite element models were designed to be simply supported with pin-roller boundary conditions and plane sections were enforced to remain plane. In addition, the results of the cambered finite element models were compared to the experimental results of cambered beams to evaluate the method used experimentally to measure residual stresses and to evaluate the plastic properties of the steel material used in the finite element models.

Time-temperature curves were generated externally from the finite element models by performing an external heat transfer analysis using the finite difference method, which is discussed in detail in Salam [13]. The accuracy of the finite difference method in modeling the temperature distribution when applying heat using an oxy-acetylene torch is discussed in Kowalkowski [5]. The finite difference approximation uses a heat balance difference equation and a finite difference mesh of the heated region. Properties to define conduction, convection, and radiation are defined in the model, which were calibrated from the work performed by Kowalkowski [5]. The results from the analysis includes time-temperature curves for all nodes of the finite difference mesh, which are implemented in the finite element models as nodal temperatures during a thermal-stress analysis.

Figures-15 and 16 show residual stresses in the web and top flange, respectively, of the W8X18 beam heat-cambered to 0.82 in. after different heating cycles. A legend is provided for the residual stresses that is common for all results (after different heating cycles) in the figure. In addition, a graph is provided above each individual finite element model screenshot that shows the location of the last heating cycle. For instance, Figures-15a and 16a show the finite element results of the residual stresses that develop in the web and the top flange of the W8X18 beam specimen after the first heating cycle. Heat was applied to location 'C', which is highlighted in red above the figures. The last Vee/strip heat location is also shown by the Vee-shaped lines or parallel lines superimposed on the figures. In both figures, longitudinal residual stresses after removing all heat from the finite element models are shown.

As shown in Figure-15, after one heating cycle (Figure-15a), high tensile residual stresses develop in the center of the web or near the center of the Vee heat. This compares well with the experimental results from Figure-9. However, compressive residual stresses develop near the bottom of the web which is dissimilar than most of the results in Figure-9. The residual stresses are often above the yield stress and significantly higher than what AISC [15] assumes for the residual stresses in design calculations. Per Figure 16a, high compressive residual stresses develop in the

flange tips that are higher than the yield stress. The flange tips cool faster than the flange around the K-region. Therefore, the flange tips want to contract upon cooling but are restricted by the rest of the cross-section causing the flange tips to yield in tension. When the entire cross-section cools, the flange tips are subjected to compressive residual stresses since they desire to be longer due to previous yielding in tension. All stresses in these localized locations are higher than the residual stresses provided in Figures-9 and 10, which are averaged over an 8 in. strip. This reveals that experimental measurements will not accurately depict the magnitude of residual stresses in localized regions unless other methods are used for measurement.

Figure-15e shows the finite element results of the web longitudinal residual stresses after the seventh and last heating cycle. After the seventh heating cycle, compressive residual stresses develop in the web below the Vee heat locations along a significant length of the beam. In spite of that, the highest magnitude of the residual stresses did not change substantially in comparison to the results after the first heating cycle. Near the last Vee heat locations, high tensile residual stresses develop near the center of the web. It appears that after each heating cycle, the residual stresses decrease in areas adjacent to where the heat was applied as if the stresses relieve somewhat. In general, the amount of heating cycles does not have a significant influence on the final maximum magnitude of residual stresses. Instead, the location of last Vee heats has the most significant influence on the residual stress distributions. At the same time, as more heating cycles are applied, a higher variation in residual stresses develop [13].

Figure-16e shows the finite element results of the top flange longitudinal residual stresses after the seventh heating cycle. The figure indicates that the maximum residual stresses after the first heating cycle are similar to the maximum residual stresses after the seventh heating cycle. Similar to after the first heating cycle, compression residual stresses develop at the flange tips due to the flange tips cooling faster than near the k-region. The residual stresses at heated regions are slightly higher than the yield stress after each heating cycle and more of the beam is subjected to high residual stresses along the entire heated region as more heating cycles are applied. High stresses appear to be somewhat relieved in areas just outside of the strip heat location.

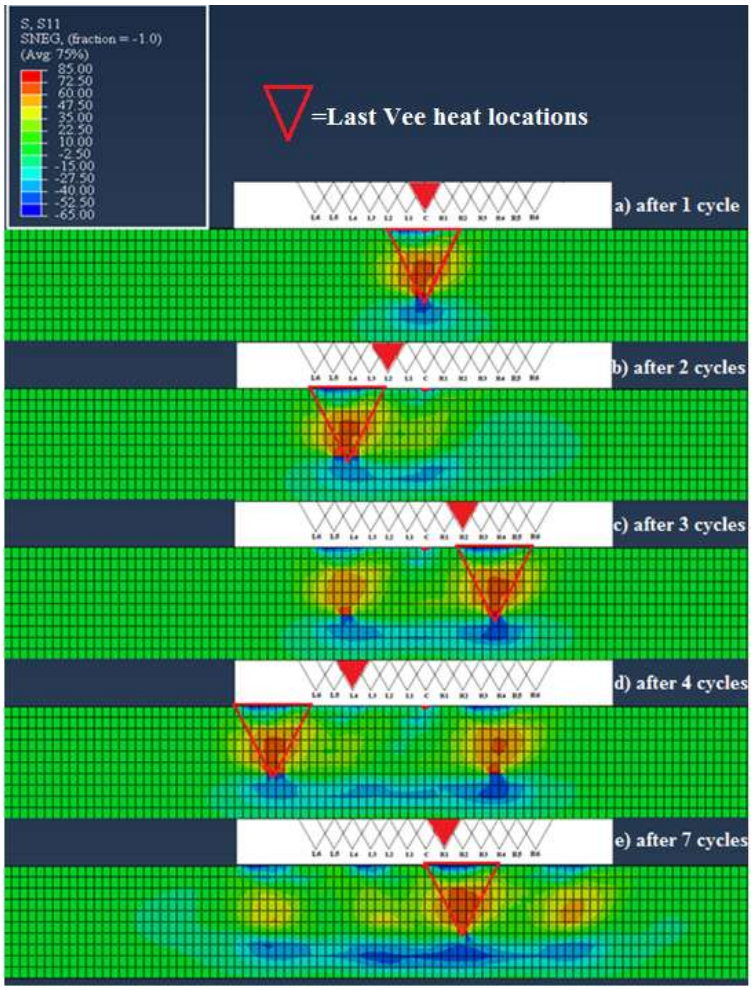

Fig-15: Web longitudinal residual stresses in the first W8X18 beam after various heating cycles

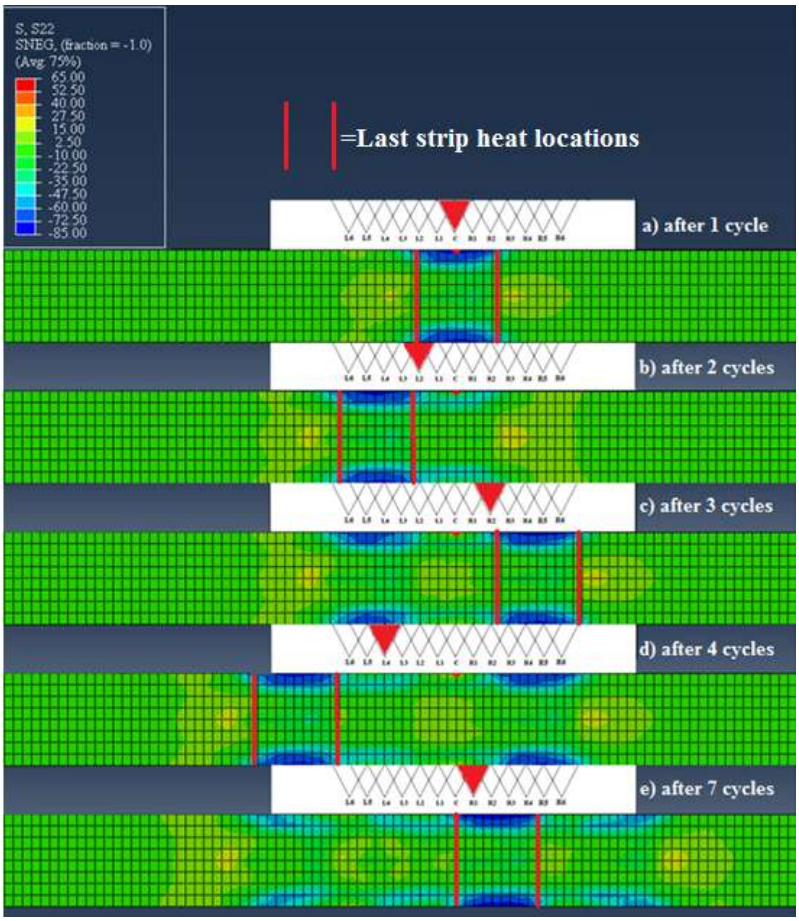

Fig-16: Top flange longitudinal residual stresses in the first W8X18 beam after various heating cycles

Figure-17 compares the total camber results obtained after each heating cycle between the experimental results and the analytical results using ABAQUS. The same locations of the heating cycles used for the experimental beams were simulated in the finite element models. In the finite element models, the beams were allowed to cool all the way to ambient temperature in between each heating cycle. In the experimental investigations, the beams were cooled to 250 ºF prior to applying the next heating cycle. Camber was measured in the finite element model as the displacement at midspan after the beam cooled. The experimental camber was measured after each heat cycle using a measuring tape. The analytical and experimental results compare well to each other, thus verifying that the heat transfer analysis using the finite difference method is acceptable when modeling steel heated with oxy-acetylene torches. In addition, the material properties at elevated temperatures appear to be defined appropriately. The slight differences between the analytical and experimental results may be linked to uncertainties in the maximum temperature during the experimental investigations. It is probable that the maximum temperature often exceeded 1200 ºF during the experimental investigations, which was mentioned for this beam in the previous section. The analytical results show a linear increase in camber indicating that approximately the same amount of camber was achieved during each heating cycle.

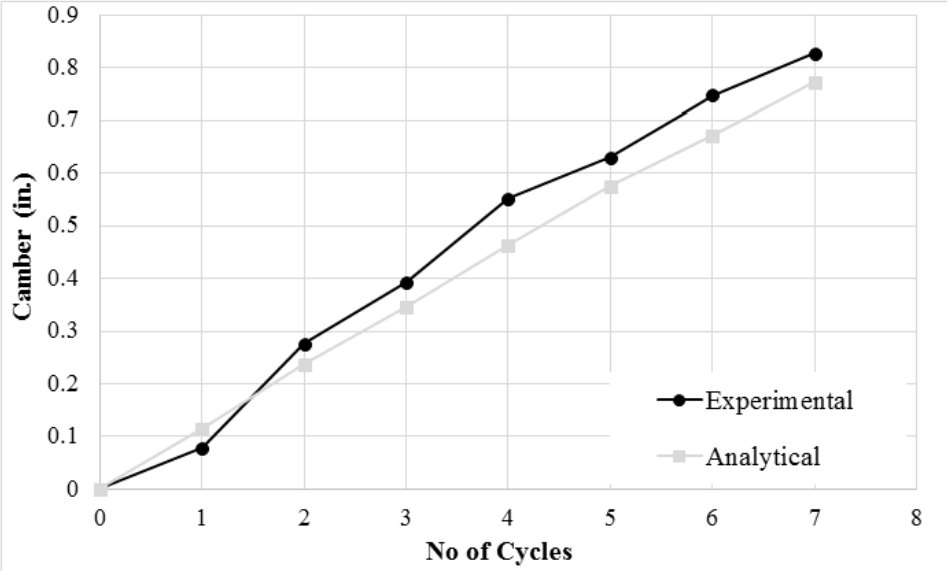

Fig-11: Analytical and experimental camber results for the first W8X18 beam

The residual stresses presented in this section for the analytical results and the previous section for experimental results are proven very high; in some cases, meeting the yield stress for heat-cambered beams. This is concerning with respect to serviceability since further applied service loads will cause premature yielding or further yielding in areas of high residual stresses. The overall amount of yielding would not occur under the same loading if the residual stresses are not present and therefore, the residual stresses may have a significant influence on the deflections for a given applied load, thus making traditional elastic equations used to solve for vertical deflections invalid. Therefore, load-displacement curves for W8X18 were developed that compare the results of cambered beams subjected to further gravity loads vs. the results of beams non-cambered and subjected to the same gravity loads. More conditions with different beam sizes and boundary conditions are discussed in detail in Salem [13].

For a simply supported W8X18 beam, a total of four cases were analyzed as described in detail in Salem [13]. Two cases were analyzed after subjecting the beam to cold-cambering with a maximum camber displacement of 0.82 in. and 1.5 in. Two cases were analyzed after subjecting the beam to heat-cambering with a maximum camber displacement of 0.82 in. and 1.5 in. After each camber, a uniform load was applied along the length of the beam and load-displacement curves were generated.

As an example, Figure-18 shows a comparison of the uniformly distributed load-displacement (at midspan) behavior between the cold-cambered and non-cambered W8X18 beams. In Figure-18, the cold-cambered beam was cambered to 1.5 in. prior to applying the uniform load. The results indicate that cold-cambering has very little influence on the load-displacement behavior of steel beams. Figures-19 shows a comparison between the load-displacement behavior at the mid-span of the heat-cambered and the non-cambered W8X18 beams. The beam was heat-cambered to 1.5 in. at midspan. The comparative results are different in comparison to the results presented for the cold-cambered beam. In general, heat-cambering has a different effect on the residual stress results and a more significant influence on the serviceability behavior. The change in initial stiffness is not particularly significant. However, the results of the heat-cambered beams show a slight reduction in load-carrying capacity in comparison to the non-cambered beam. In all models, the beam was subjected to displacement until the program terminated. After further inspection, it was concluded that the analysis of heat-cambered beams terminated prematurely when some of the cross-section reached the ultimate stress and therefore, lower deflections were reached. However, the measured deflection is well beyond expected deflection under service loads. The heat-cambered models terminated prematurely in comparison to the non-cambered model and the cold-cambered model; hence, part of the cross-section reaches high stresses quicker. Figures-18 and 19 also show the equivalent uniform load that is required to reach the theoretical plastic moment capacity of the steel beam. This is identified as “Plastic Uniform Load). In addition, Figures-18 and 19 show the uniform load that would be considered the maximum service load that the beam would be subjected during its service life. This is identified as “Uniform Service Load”. The service load is computed as the plastic uniform load multiplied by the strength reduction factor of 0.9 and divided by factor of safety of 1.5. An average, AISC assumes that ultimate loads are 1.5 times higher than service loads. All the load-displacement relationships

show negligible change in elastic behavior near service load limits. This verifies that traditional elastic equations used to calculate beam deflections and rotations are still valid after cambering. This discussion is valid for additional studies performed in Salem [13] when evaluating the effects of residual stresses on the serviceability of steel beams.

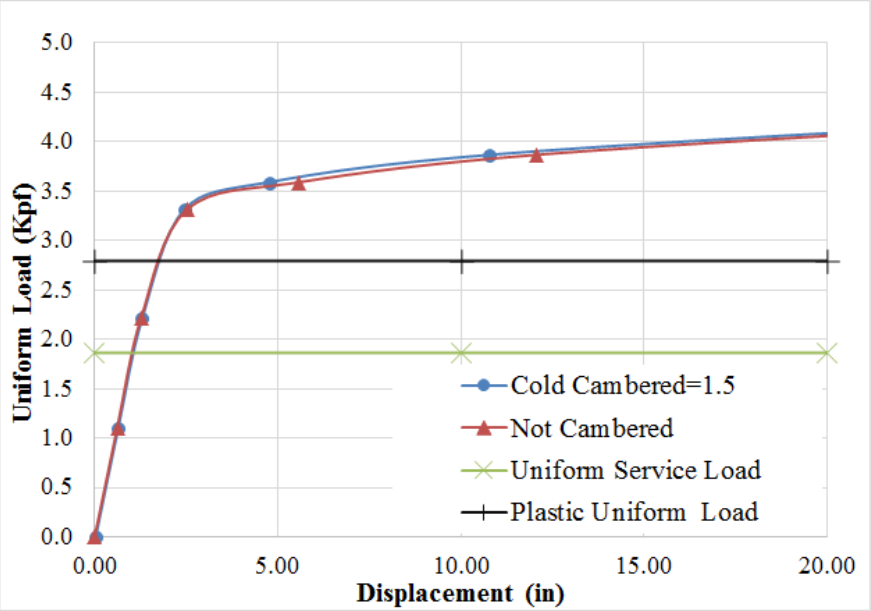

Fig-12: Load-displacement of W8X18-CC-1.5-PP and non-cambered beams

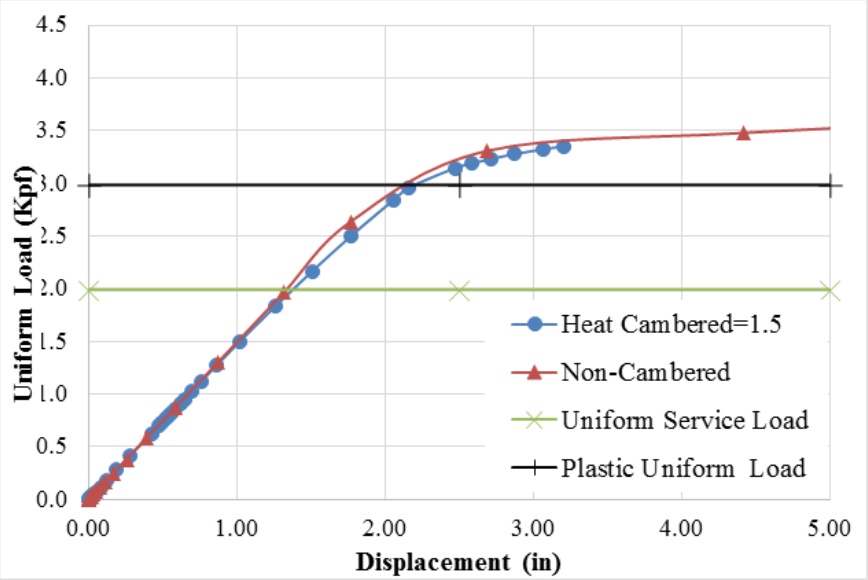

Fig-19: Load-displacement of W8X18-HC-1.5-PP and non-cambered beams

SUMMARY AND RECOMMENDATIONS

The effects of cambering on the residual stresses and structural performance of steel beams were evaluated. The results of the heat-cambered beams as opposed to cold-cambered beams were the focus of this paper. Effects were evaluated both experimentally and analytically. Experimentally, heat-cambering was used to camber three steel beams. Two different steel shapes and two different magnitudes of camber were considered. The results indicate that high compressive residual stresses develop in the flanges, particularly at the flange tips, which are often higher than the yield stress. In addition, high tensile residual stresses develop in the web, which are highest in magnitude near the center of the web or close to the apex of the Vee heat. However, the results are sometimes sporadic which may be related to; the stresses are averaged over 8 in. lengths within strips, non-uniform heat, and the number of heating cycles applied to specific Vee/strip heat locations.

Analytically, the results indicate that even higher residual stresses develop at more localized locations along the length of the beam. The residual stresses often exceed the yield stress. However, the stress results are localized and therefore, do not have a significant influence on the structural behavior of the beam even if nonlinearity develops at the early stages of loading [13]. This was determined by comparing load-displacement results of non-cambered and heat-cambered beams and also evaluating the lateral-torsional buckling capacity of non-cambered and heat-cambered beams using finite elements. These results are presented elsewhere [13]. In general, the results of this research investigation did not find any significant reasons that heat-cambering cannot be employed as the method to camber beams. Heat-cambering can be idealized for various boundary conditions and various steel cross-sections.

REFERENCES

1. Gergess AN, Sen R. Cambering structural steel I-girders using cold bending. Journal of Constructional Steel Research. 2008 Apr 1;64(4):407-17.
2. Ricker DT. Cambering steel beams. Engineering journal-american institute of steel construction inc. 1989 Jan 1;26(4):136-42.
3. Downey EW. Specifying camber. Modern Steel Construction. 2006 Jul;46(7):53.
4. Roeder CW. Experimental study of heat induced deformation. journal of structural Engineering. 1986 Oct;112(10):2247-62.
5. Kowalkowski KJ. Effects of multiple damage-heat straightening repair cycles on the structural properties and serviceability of steel beam bridges; 2005.
6. Holt JE. Flame straightening: a friend in need. Welding Engr.. 1955 Oct;40(10):44-6.
7. Ditman O. *Determination of thermal shrinkage in structural steel* (Doctoral dissertation, University of Washington).
8. Chin W, W.. Linear shrinkage of steel. MScCE thesis, U. of Washington, Seattle, Wash. 1962.
9. Holt RE. Flame straightening basics. Welding Engineer. 1965 Sep;50(9):49-53.
10. Roeder CW. Use of thermal stress for seismic damage repair. Final Report on NSF Grant CEE-82. 1985 Oct;5260.
11. Avent RR, Robinson PF, Madan A, Shenoy S. Development of engineering design procedures for heat-straightening repair of damaged structural steel in bridges. Final report. 1992 Dec.
12. Avent RR, Mukai DJ, Robinson PF. Residual stresses in heat-straightened steel members. Journal of materials in civil engineering. 2001 Feb;13(1):18-25.
13. Salem S. ‘‘Effects of Heat Cambering on Residual Stresses and Structural Performance of Steel Beams.’’ PhD dissertation, Dept. of Civil Engineering, Lawrence Tech University; 2018.